Electronic Supplementary Information

A new near-infrared phosphorescent iridium(III) complex conjugated to an xanthene dye for mitochondria-targeted photodynamic therapy

Yongquan Wu,[a,b,c] Jie Wu[c] and Wai-Yeung Wong[a,b]*

[a]Department of Applied Biology and Chemical Technology, The Hong Kong Polytechnic University, Hung Hom, Hong Kong, P. R. China, E-mail: wai-yeung.wong@polyu.edu.hk

[b]The Hong Kong Polytechnic University Shenzhen Research Institute, Shenzhen518057, P. R. China

[c] Key Laboratory of Organo-Pharmaceutical Chemistry of Jiangxi Province, Gannan Normal University, Shiyuan South Road, Ganzhou 341000, P. R.China

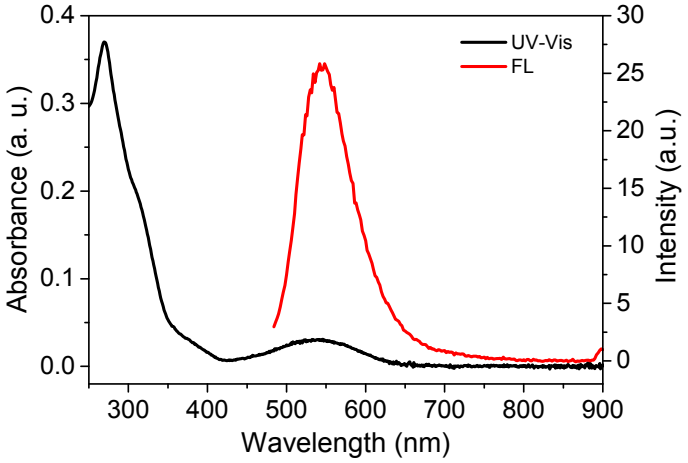

Fig. S1 The absorption and fluorescence spectra of XE-P.

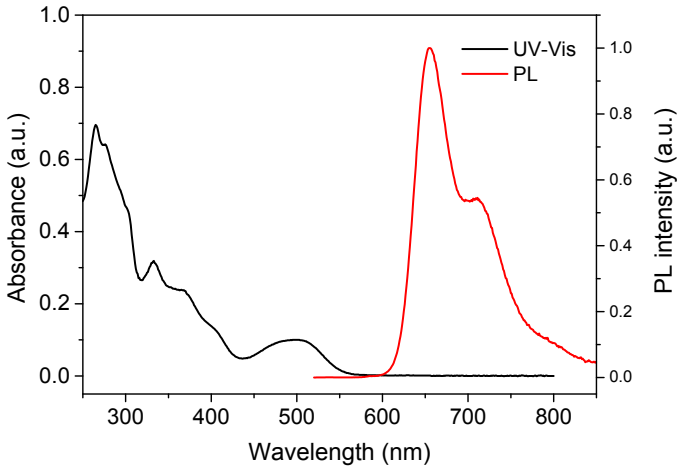

Fig. S2 The absorption and phosphorescence spectra of NIR-Ir-bpy.

Table S1. Comparison of representative Ir(III) photosensitizers (complexes or the corresponding nanomaterials) for imaging and PDT

Selected reference	λ_{ex}&λ_{em}/nm	Yield of $^1O_2$	Imaging applications	PDT applications
This work	532/650	0.71	Mitochondria	Cells and in vivo
Dalton Trans. 2020, **49**, 3562.	425(800)/570	0.94	Mitochondria	Cells
Inorg. Chem. 2020, **59**, 14796.	467(800)/570	0.31	Mitochondria	Cells
Nano Lett. 2020, **20**, 6526.	540/720	0.53	*In vivo* imaging	Cells and in vivo
Adv. Sci. 2019, 6, 1802050.	469/671	Not given	Not given	Cells and in vivo
Angew. Chem. Int. Ed. 2019, **58**, 6311	561/660	Not given	Not given	Cells
Chem. Sci.2019, 10, 5085.	488/>650	0.97	Lifetime imaging	Cells and in vivo
ACS Appl. Mater. Interfaces 2019, **11**, 15276.	420/545	0.54	Mitochondria	Cells and in vivo
ACS Appl. Mater. Interfaces 2019, **11**, 8797.	550/630	0.43	Mitochondria	Cells and in vivo
Chem. Eur. J. 2019, **25**, 7948.	400/520	0.47	Mitochondria	Cells
Chem. Eur. J. 2018, **24**, 10999.	465/620	0.71 (pH=4)	Lysosome	Cells
Chem. Eur. J. 2018, **24**, 4607.	380/595	Not given	Endoplasmic reticulum	Cells
Chem. Sci., 2015, **6**, 5409	405/576	0.51	Lysosome	Cells

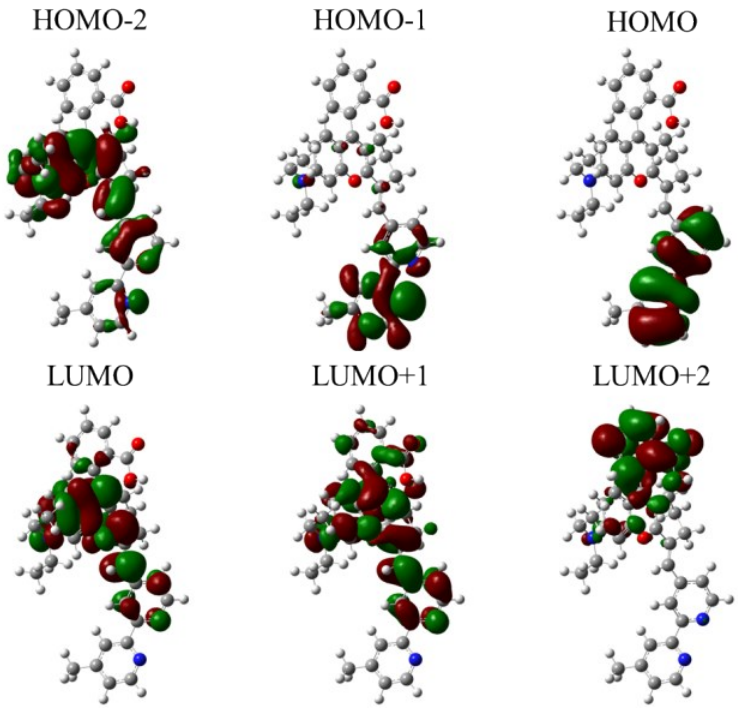

Fig. S3 Representations of the frontier molecular orbitals (MOs) for the S_0 geometry of XE-P at the DFT//B3LYP/6-31G* level.

Table S2. Energies of the frontier molecular orbitals (in eV) calculated at the B3LYP/[LANL2DZ-ECP/6-31G*]

Sample	HOMO-2	HOMO-1	HOMO	LUMO	LUMO+1	LUMO+2	GAP
XE-P	-8.59	-8.41	-8.40	-5.85	-4.16	-4.03	2.55
NIR-Ir-XE	-9.52	-9.12	-8.85	-7.47	-6.35	-5.83	1.38

TableS3. Vertical absorption energies and the corresponding oscillator strengths obtained from TD-DFT calculations at the B3LYP/[LANL2DZ-ECP/6-31G*] level. The absorption energies are based on the optimized S_0 geometry.

Sample	S-linked	Energy	$\lambda_{abs.}$	*f* (oscillator strengths)
NIR-Ir-XE	$S_0 \rightarrow S_1$	1.02 eV	1219.3 nm	0.0248
	$S_0 \rightarrow S_2$	1.22 eV	1016.8 nm	0.0070
	$S_0 \rightarrow S_3$	1.72 eV	720.9 nm	0.0011
	$S_0 \rightarrow S_4$	1.86 eV	666.9 nm	0.0016
	$S_0 \rightarrow S_5$	1.91 eV	648.4 nm	0.0036
	$S_0 \rightarrow S_6$	2.10 eV	591.8 nm	0.0004
	$S_0 \rightarrow S_9$	2.47 eV	502.8 nm	0.4364

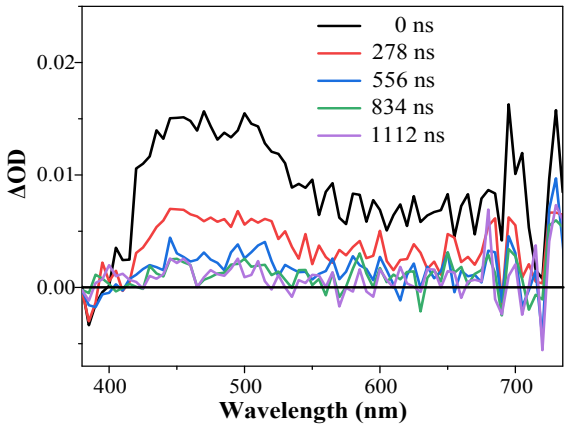

Fig. S4 Transient absorption spectra of NIR-Ir-XE in degassed toluene after irradiated by the pump light at 355 nm, from 278 ns to 1112 ns.

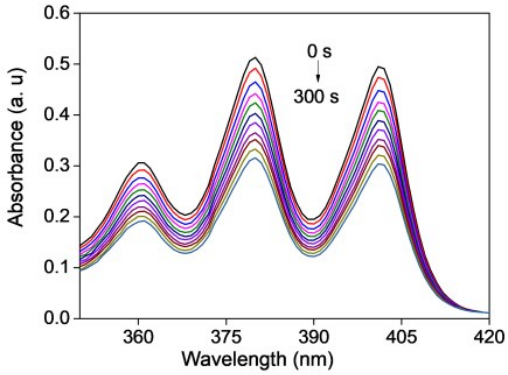

Fig. S5 The decomposition rates of ABDA by rose benga (RB); A_0 and A are the absorbance of ABDA in the presence of the photosensitizers at 532 nm before and after irradiation, respectively. The absorbance value of RB at 532 nm is 0.113.

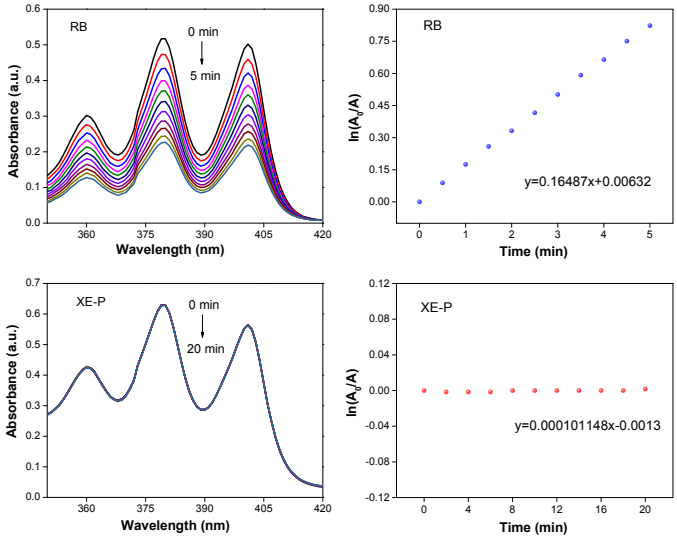

Fig. S6 The decomposition rates of ABDA by rose bengal (RB) and XE-P, A_0 and A are the absorbance of ABDA in the presence of the photosensitizers at 532 nm before and after irradiation, respectively. The absorbance value of RB and XE-P at 532 nm is 0.121 and 0.186, respectively.

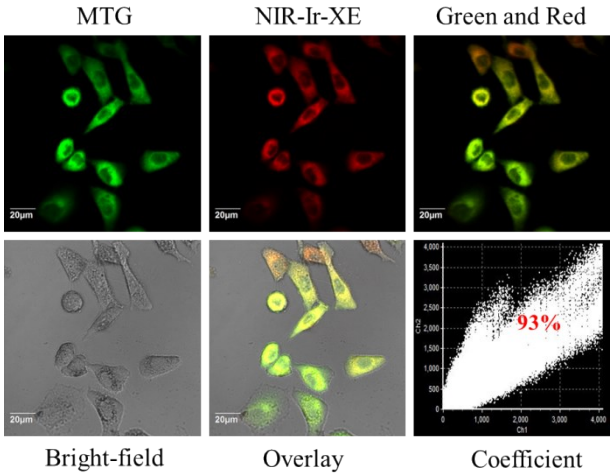

Fig. S7 Confocal images of MCF-7 cells with the incubation of NIR-Ir-XE (5 μM) for 30 minutes followed by co-staining with Mito-Tracker Green FM (MTG, 100 nM) for 30 min. (a) green channel of MTG; (b) Red channel of NIR-Ir-XE; (c) overlaid of green and red channels; (d) bright-field; (e) overlaid of green, red, and bright-field channels; (f) Pearson's correlation coefficients of green and red channels. Imaging conditions: Green channels of MTG, λ_{ex} = 488 nm, λ_{em} = 505–550 nm; red channels of NIR-Ir-XE, λ_{ex} = 532 nm, λ_{em} = 630 – 730 nm.

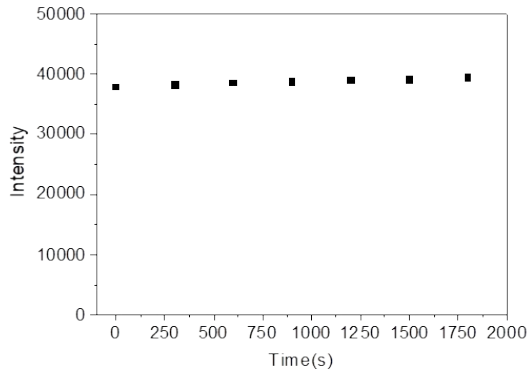

Fig. S8 Changes of luminescence intensity of NIR-Ir-XE (10 μM in ethanol) irradiated at 500 nm for 30 min.

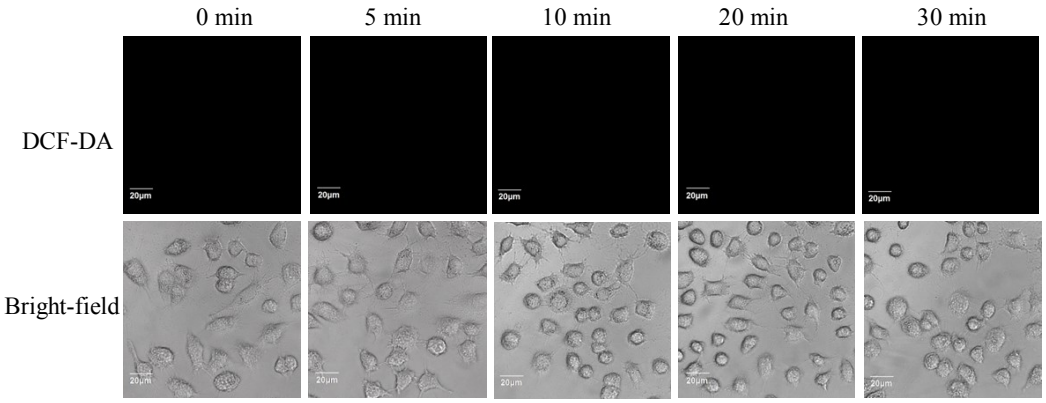

Fig. S9 ROS generation in MCF-7 cells without NIR-Ir-XE. Confocal laser scanning microscopy images showing the ROS generation in MCF-7 cells with light irradiation (0 to 30 min) after treatment with DCF-DA. The green fluorescence is from DCF-DA (λ_{ex} = 488 nm, λ_{em} = 505 – 525 nm).

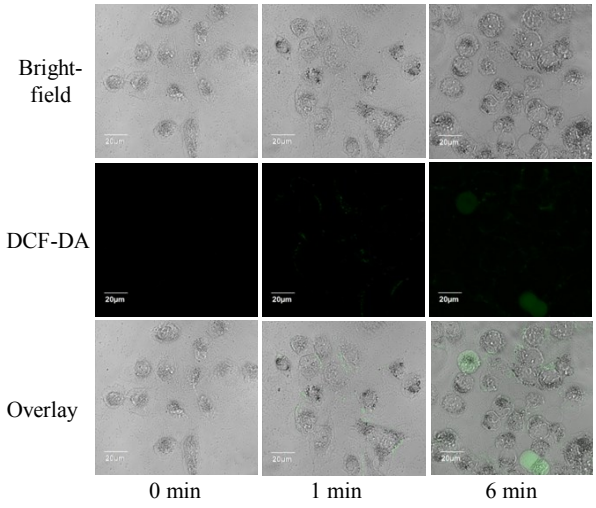

Fig. S10 ROS generation in MCF-7 cells with NIR-Ir-bpy (5 μM). Confocal laser scanning microscopy images showing the ROS generation in MCF-7 cells with light irradiation (0, 1, and 6 min) after treatment with DCF-DA. The green fluorescence is from DCF-DA (λ_{ex} = 488 nm, λ_{em} = 505 – 525 nm).

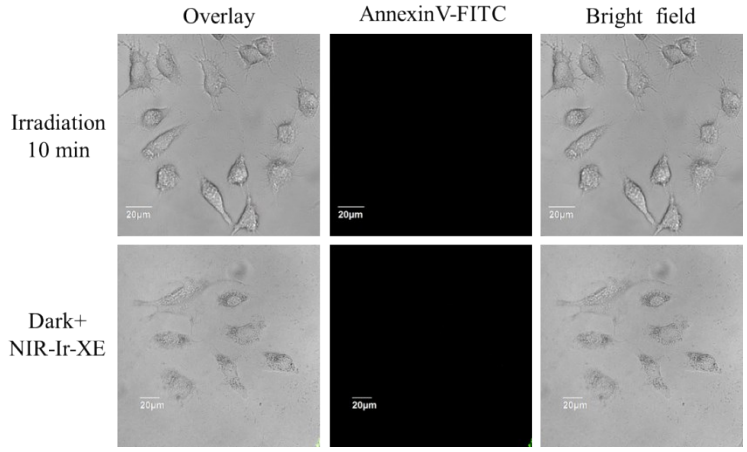

Fig. S11 Apoptosis development in MCF-7 cells without NIR-Ir-XE or without light irradiation. Imaging conditions: Fluorescein isothiocyanate (FITC)-tagged Annexin V, λ_{ex} = 488 nm, λ_{em} =510 – 540 nm.

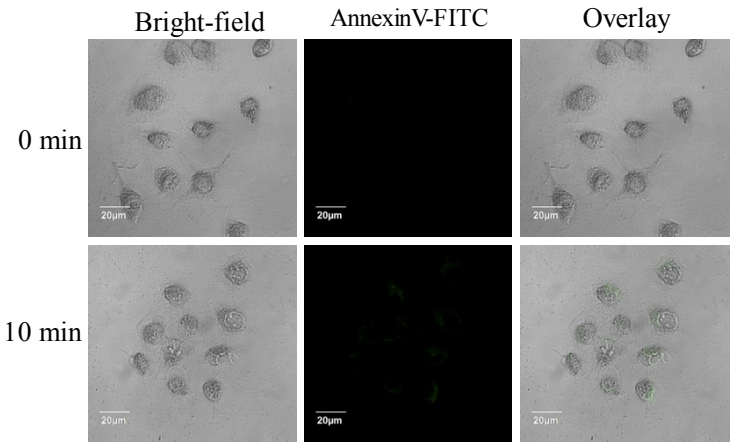

Fig. S12 Apoptosis development in response to PDT of NIR-Ir-bpy. MCF-7 cells incubated with NIR-Ir-bpy (5 μM) were irradiated for 10 min. Imaging conditions: Fluorescein isothiocyanate (FITC)-tagged Annexin V (λ_{ex} = 488 nm, λ_{em} = 510 – 540 nm).

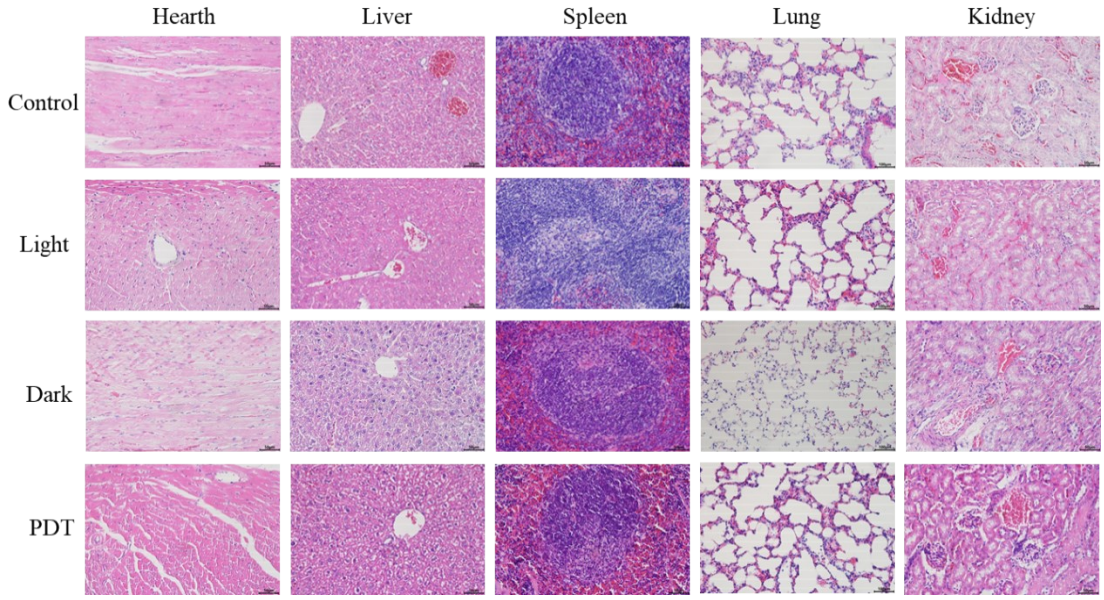

Fig. S13 H&E-stained tissue sections harvested from mice after 14 days treatments. No noticeable abnormality was observed in major organs including liver, spleen, heart, lung, and kidney.

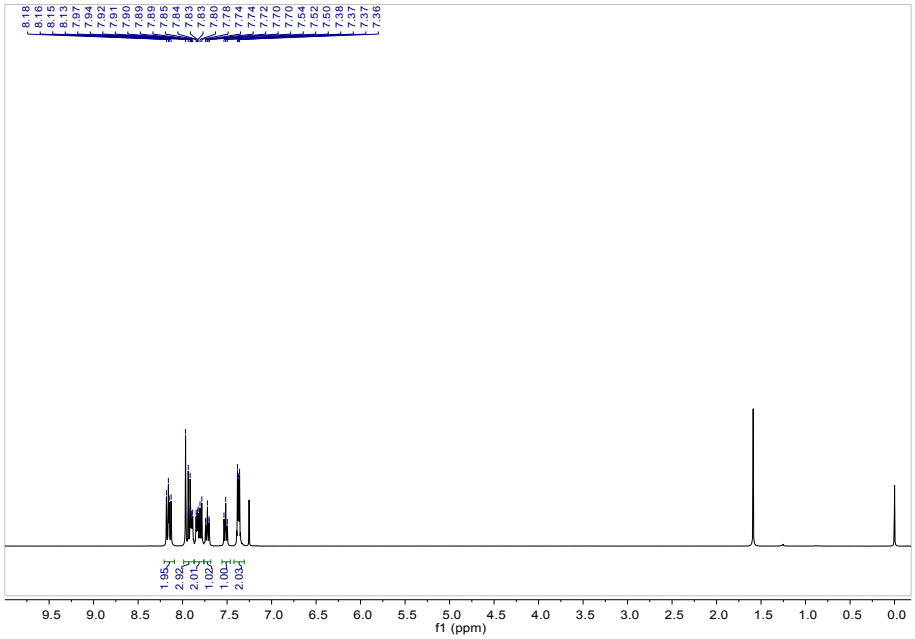

Fig. S14 ^{1}H NMR spectrum of ligand Hbtpq in $CDCl_3$.

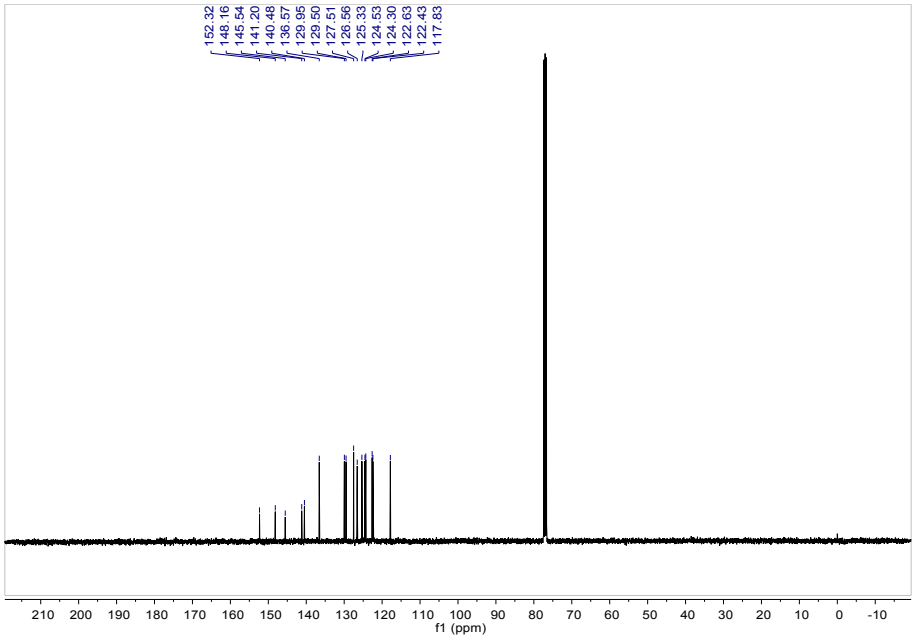

Fig. S15 ^{13}C NMR spectrum of ligand Hbtpq in $CDCl_3$.

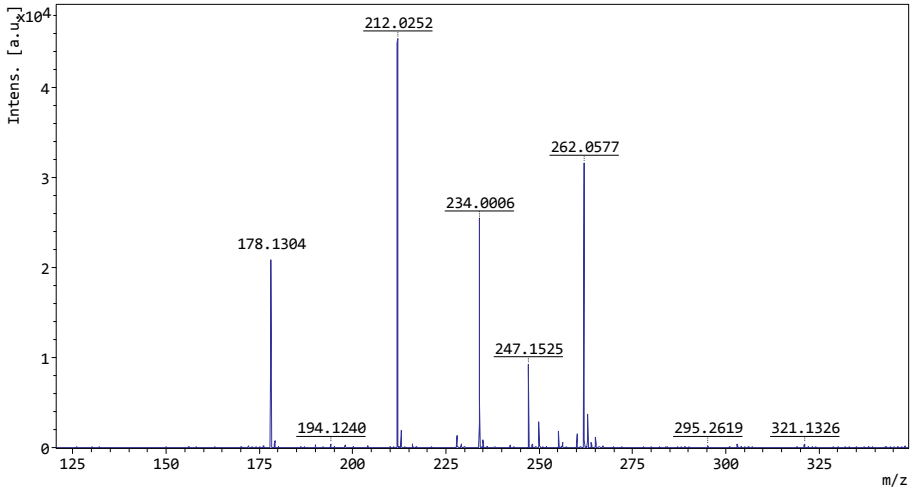

Fig. S16 MALDI-TOF-MS of ligand Hbtpq.

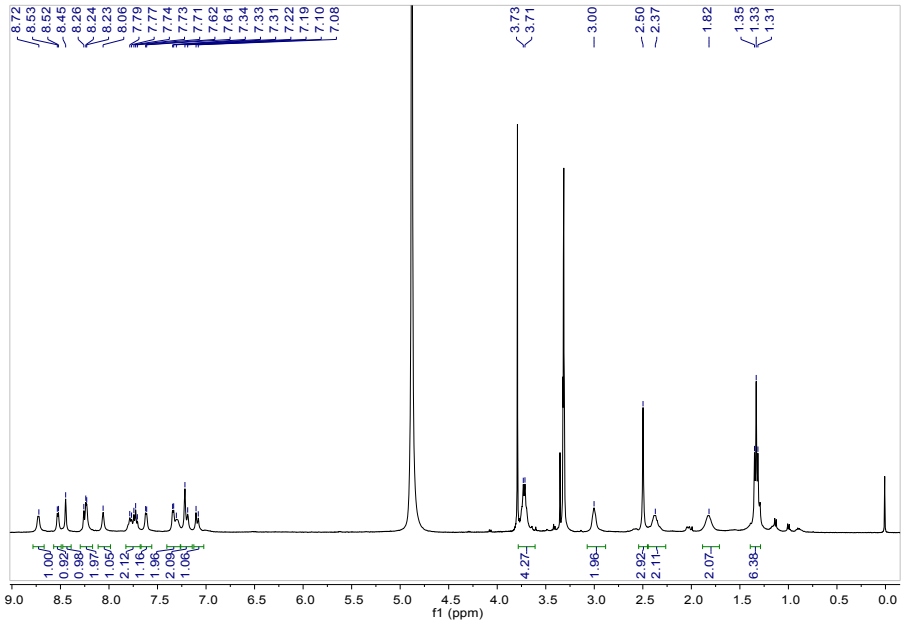

Fig. S17 ^{1}H NMR spectrum of ligand XE-P in CD_3OD.

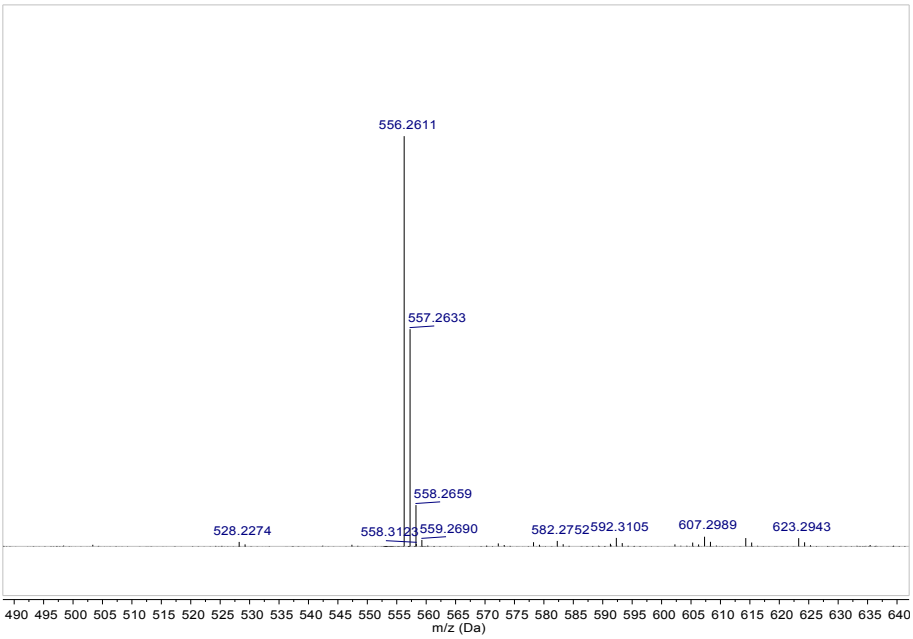

Fig. S18 HR-MS of ligand XE-P.

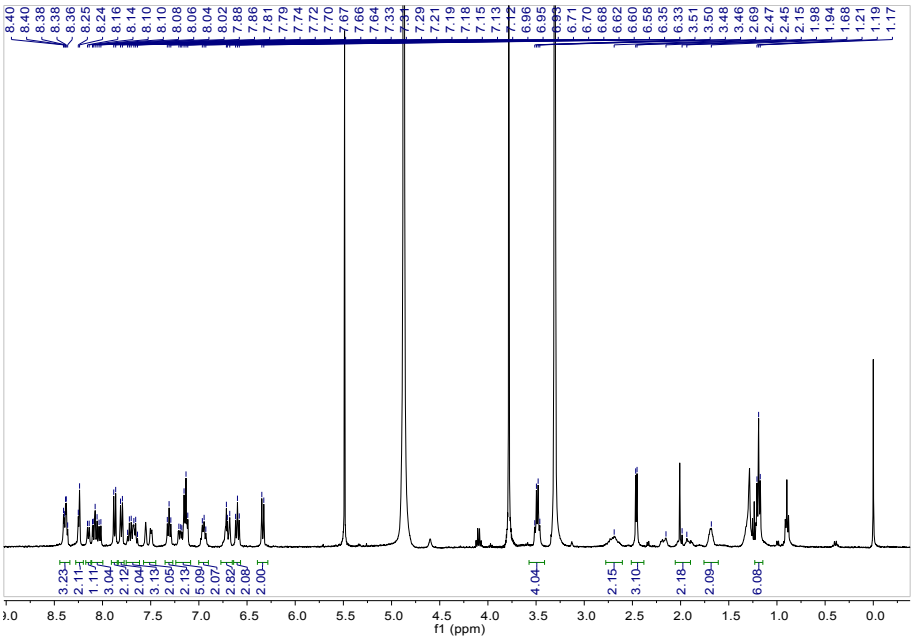

Fig. S19 ^{1}H NMR spectrum of NIR-Ir-XE in CD_3OD.

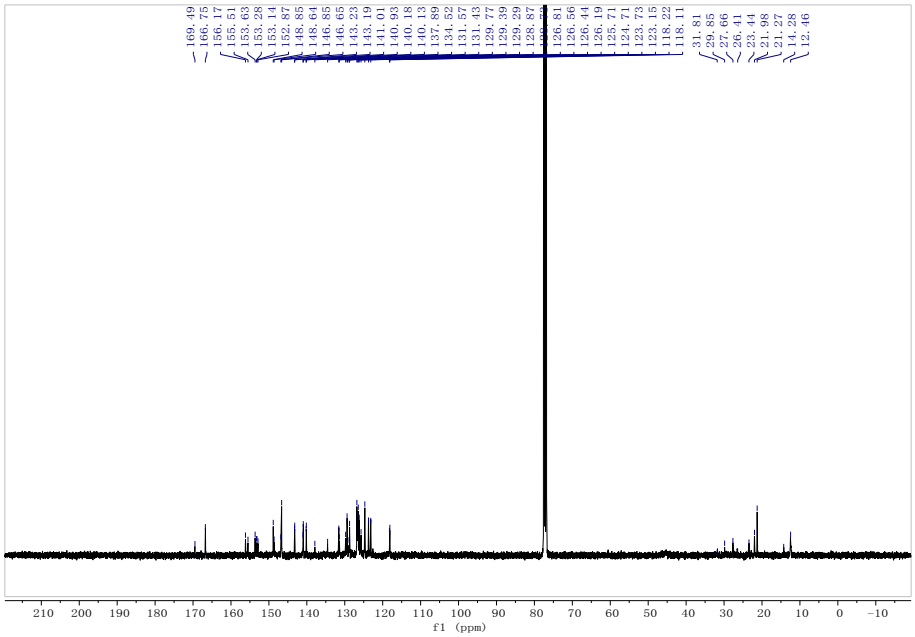

Fig. S20 ^{13}C NMR spectrum of NIR-Ir-XE in CD_3OD.

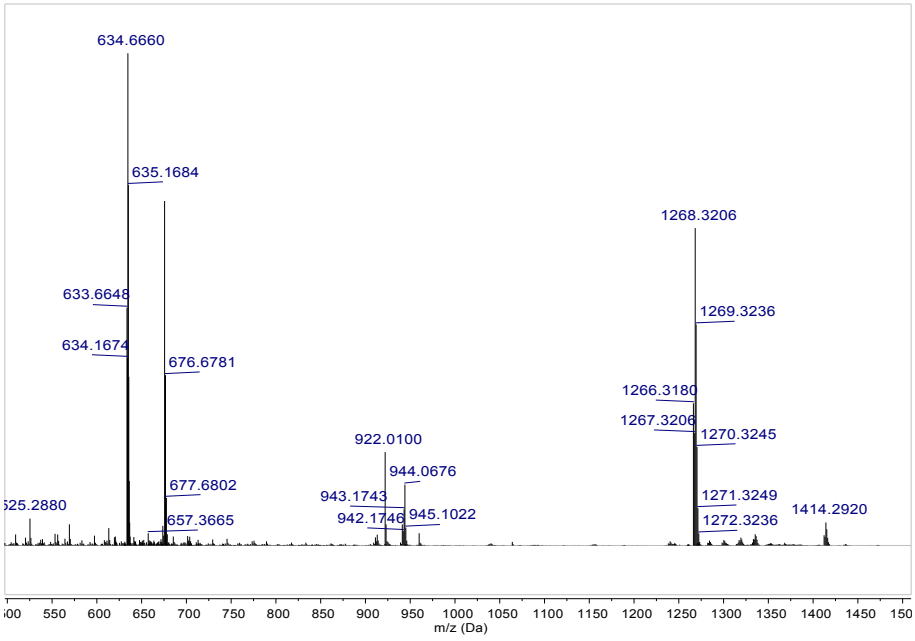

Fig. S21 HR-MS of complex NIR-Ir-XE.

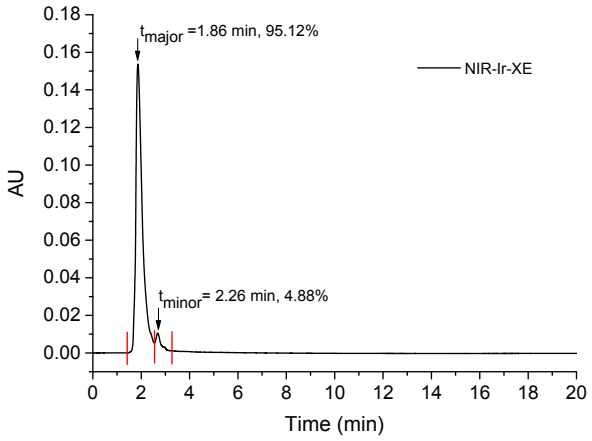

Fig. S22 HPLC analysis of complex NIR-Ir-XE.

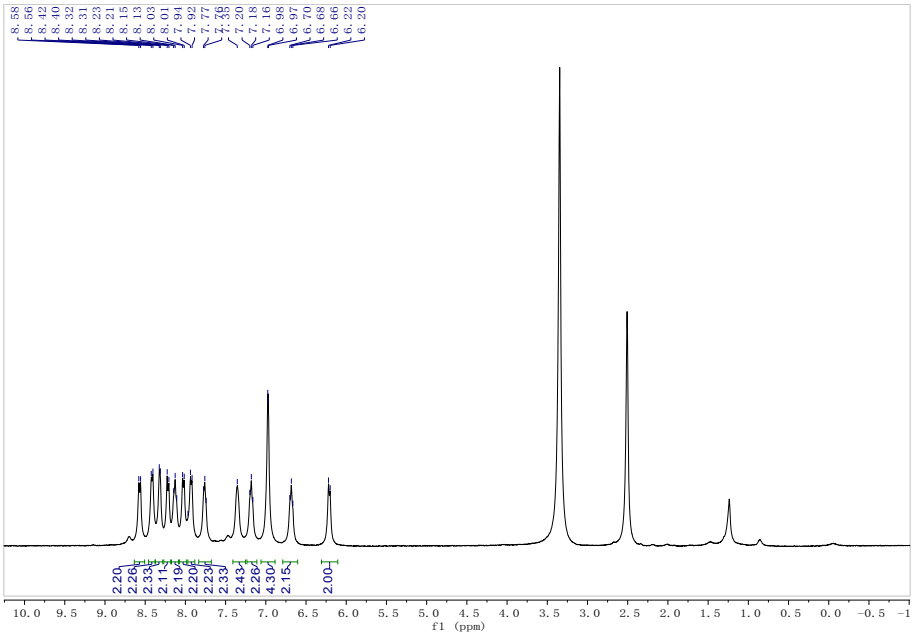

Fig. S23 ^{1}H NMR spectrum of complex NIR-Ir-bpy in DMSO-d_6.

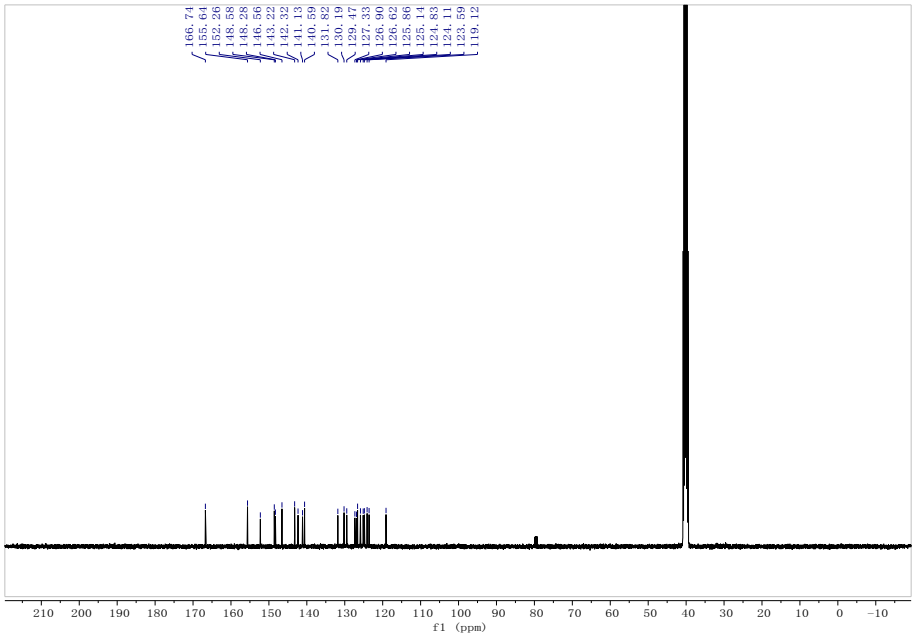

Fig. S24 ^{13}C NMR spectrum of complex NIR-Ir-bpy in DMSO-d_6.

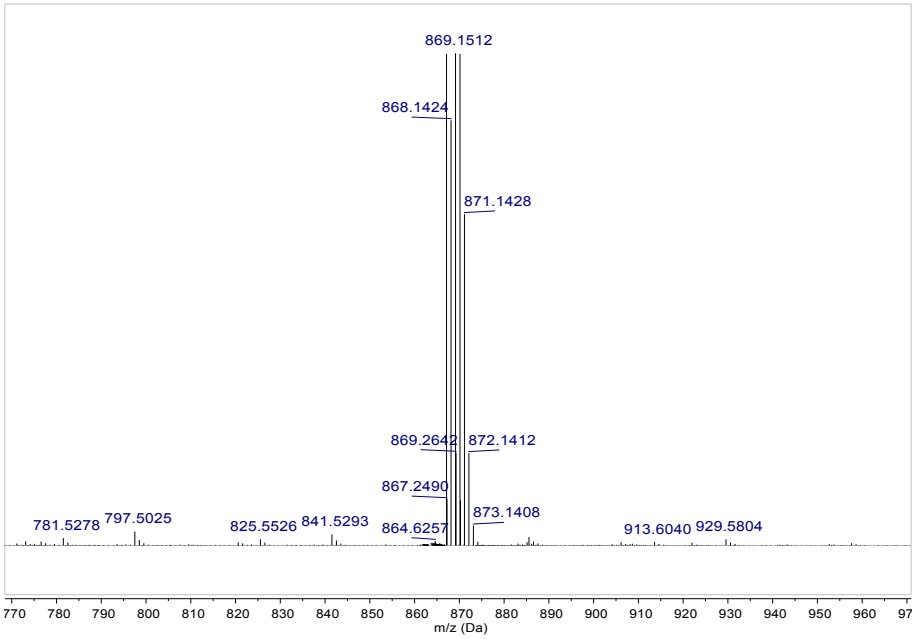

Fig. S25 HR-MS of complex NIR-Ir-bpy.